# Improvement of magnetic properties of granular perpendicular recording media by using a fcc nonmagnetic intermediate layer with stacking faults



doi: 10.1063/1.2424280

# Improvement of magnetic properties of granular perpendicular recording media by using a fcc nonmagnetic intermediate layer with stacking faults

Atsushi Hashimoto,[a] Shin Saito, and Norikazu Itagaki
*Department of Electronic Engineering, Tohoku University, 6-6-05 Aoba, Aramaki, Aoba-ku, Sendai 980-8579, Japan*

Migaku Takahashi
*Department of Electronic Engineering, Tohoku University, 6-6-05 Aoba, Aramaki, Aoba-ku, Sendai 980-8579, Japan and New Industry Creation Hatchery Center, Tohoku University, 6-6-10 Aoba, Aramaki, Aoba-ku, Sendai 980-8579, Japan*

(Received 27 June 2006; accepted 21 November 2006; published online 28 December 2006)

Various binary systems are investigated as face-centered cubic (fcc) bases for the nonmagnetic intermediate layer (NMIL) in granular perpendicular recording media. Loss of stacking order on the (111) plane in fcc NMIL is found to enhance the perpendicular magnetic anisotropy energy ($K_u^{RL}$) of the overlying medium. One persuasive reason for this enhancement is the preferred epitaxial growth of magnetic grains on only the (111) atomic terrace of the fcc NMIL due to collapse of the sixfold symmetry of $(\bar{1}11)$, $(1\bar{1}1)$, and $(11\bar{1})$ atomic terraces of the fcc NMIL. © *2006 American Institute of Physics*. [DOI: 10.1063/1.2424280]

Perpendicular magnetic recording media presently consist of three functional parts: a soft magnetic underlayer, a nonmagnetic intermediate layer (NMIL), and a recording layer (RL). Granular materials consisting of Co-base magnetic grains with oxide-rich eutectic grain boundaries are widely used for the RL, and the NMIL plays an important role in controlling the structure of such a RL by providing nuclei sites for the growth of magnetic grains in the RL, and by promoting epitaxial growth of the magnetic grains in the RL to afford a *c*-plane sheet texture. Ruthenium with such a *c*-plane orientation and rough surface is widely used as an NMIL material.[1,2] However, due to the need for high gas pressures in the sputtering of thick Ru layers, it is imperative that an alternative to Ru be identified for this application. In this letter, a guide for face-centered cubic (fcc) NMIL material design is proposed, focusing on the conditions required for epitaxial growth of the magnetic grains with *c*-plane sheet texture.

All samples prepared in the present study were fabricated by direct-current magnetron sputtering onto crystalline glass substrates at room temperature. The NMIL was deposited on a 20-nm-thick $(Ni_{81}Fe_{19})_{54}Cr_{46}$ seed layer.[3] NMIL was cosputtered with a fcc metal and additional metal targets under Ar (gas pressure, 0.6 Pa). The alloy composition of the NMIL was controlled by adjusting the discharge power for each target. The thickness of the NMIL was fixed at 20 nm. The granular RL was subsequently sputtered from a $Co_{74}Pt_{16}Cr_{10}$−8 mol % $SiO_2$ target. The composition of the NMIL alloy was checked by x-ray fluorescence analysis, and the crystalline structure was examined by in-plane x-ray diffractometry (XRD) using Cu $K\alpha$ radiation and transmission electron microscopy (TEM). The incident angle of x rays in XRD was fixed at 0.4°, and thus the profiles reflect the structural information at a depth of approximately 20 nm from the film surface. The magnetic properties were measured using polar Kerr equipment (PKE), a vibrating sample magnetometer, and a torque magnetometer. The averaged uniaxial magnetic anisotropy with respect to the RL normal ($K_u^{RL}$) was derived by perpendicular magnetic torquemetry.[4]

To obtain *c*-plane-oriented Co-base magnetic grains with a hexagonal close packed (hcp) structure by epitaxial growth on the NMIL, it is important to achieve precise control of both the wettability of magnetic grains on the NMIL and the lattice match between magnetic grains and the NMIL material. In the present study, fcc metals such as Pd, Ir, Pt, Au, and Ni were chosen as base materials for the NMIL, as these materials have a close packed atomic plane of (111) with sixfold-symmetric atomic arrangement. To allow the wettability and lattice constant of the NMIL to be changed continuously, Ti, Cr, Zr, and Nb were chosen as additional materials, all of which have a wide solution range in the host fcc metals at high temperature.

Figure 1 shows the dependence of coercivity ($H_c$) and loop squareness (Sq) on Cr content (measured by PKE) for glass/NiFeCr(20 nm)/NMIL(20 nm)/RL(16 nm) films with (a) Ir–Cr, (b) Pd–Cr, (c) Au–Cr, and (d) Pt–Cr as the NMIL materials. In the Ir–Cr system, $H_c$ and Sq increase from 0.6 kOe and 0.4 at 0 at. % Cr, to 2.2 kOe and 1.0 at 40 at. % Cr, above which $H_c$ and Sq remain nearly constant to 65 at. % Cr then degenerate abruptly. The magnetic hysteresis with the applied field oriented toward the film normal is thus enhanced at intermediate composition ranges ( 40–65 at. % Cr), as also observed for the Pd–Cr, Au–Cr, and Pt–Cr systems. The composition ranges yielding enhanced $H_c$ and Sq are 20–40 at. % Cr for the Pd–Cr system, 20–60 at. % Cr for Au–Cr, and 20–65 at. % Cr for Pt–Cr [see Figs. 1(b)–1(d)]. The highest value of $H_c$ obtained in the present study was 3.1 kOe, obtained for the Pt–Cr system with Sq=1.0 at 45 at. % Cr.

Table I lists the $K_u^{RL}$ for the present films, along with the properties of Ir, Pd, Au, Pt, and Ru NMILs. The addition of Cr to the fcc NMIL leads to an increase in $K_u^{RL}$ of the over-

[a]Electronic mail: a-hashi@ecei.tohaku.ac.jp

 

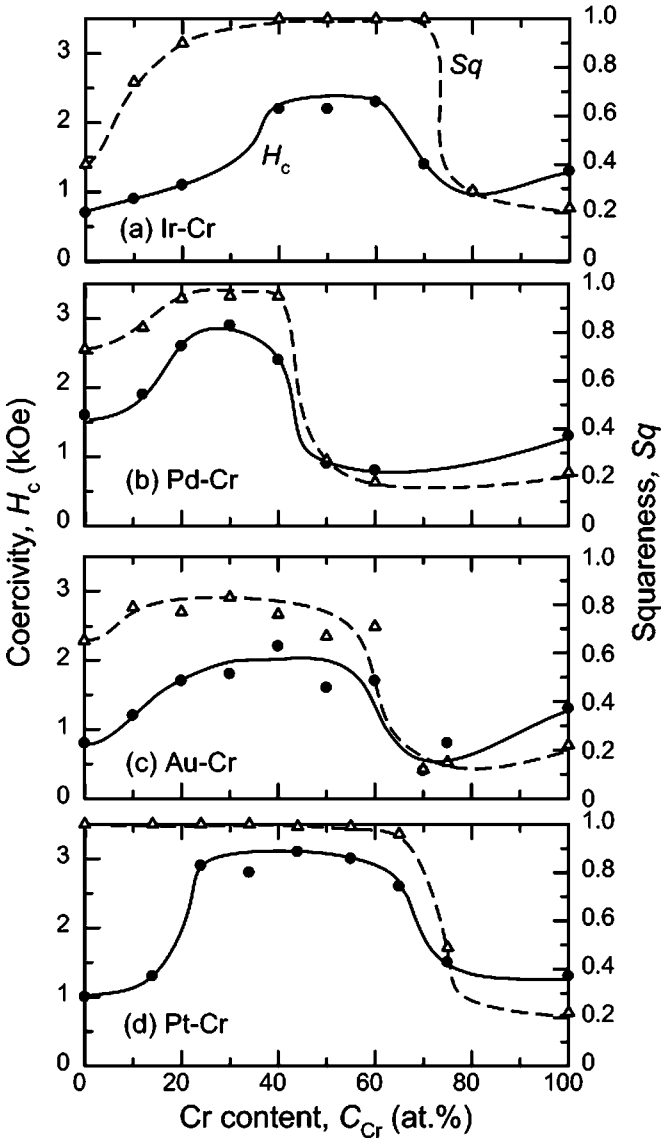


FIG. 1. Dependence of $H_c$ (solid line) and Sq (broken line) on Cr content of NMIL for glass/NiFeCr(20 nm)/NMIL(20 nm)/CoPtCr–$SiO_2$(16 nm) film with (a) Ir–Cr, (b) Pd–Cr, (c) Au–Cr, or (d) Pt–Cr NMIL.

lying RL, the $H_c$ and Sq of which are improved as shown in Fig. 1. This result suggests that the increase in $H_c$ and Sq achieved by Cr addition to fcc NMIL is related to an increase in $K_u^{RL}$ of the overlying RL.

Figure 2 shows in-plane XRD profiles for the Ir–Cr and Pt–Cr NMIL systems over the full range of Cr content. On the basis of out-of-plane XRD analysis accounting for the crystal lattice geometry and (111) sheet texture of the layer, the diffraction line near $2\theta_\chi=68°$ ($D_h$) is considered to correspond to the (220) plane of (111)-oriented NMIL grains. With increasing Cr content, the position of $D_h$ shifts gradually to higher angles. Diffraction lines due to the (110) and (200) planes originating from the Cr-base body-centered cubic (bcc) phase emerge as the Cr content exceeds 80 at. % in

TABLE I. Cr content of NMIL and $K_u^{RL}$ for glass/NiFeCr(20 nm)/NMIL(20 nm)/CoPtCr–$SiO_2$(16 nm) films.

| NMIL material | Ir–Cr | | Pd–Cr | | Au–Cr | | Pt–Cr | | Ru |
|---|---|---|---|---|---|---|---|---|---|
| Cr content (at. %) | 0 | 50 | 0 | 30 | 0 | 50 | 0 | 34 | ··· |
| $K_u^{RL}$ ($10^6$ ergs/cm$^3$) | 3.2 | 4.0 | 2.9 | 3.8 | 3.5 | 4.5 | 2.9 | 4.3 | 4.6 |

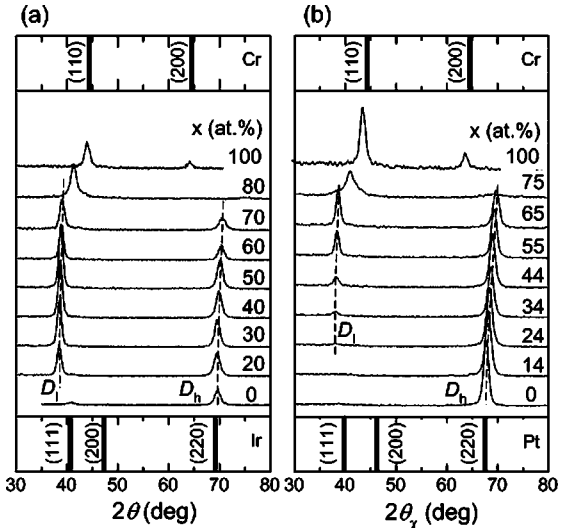


FIG. 2. In-plane XRD profiles for (a) NiFeCr(20 nm)/$Ir_{100-x}Cr_x$(20 nm) and (b) NiFeCr(20 nm)/$Pt_{100-x}Cr_x$(20 nm) NMIL films with various Cr contents.

the Ir–Cr system and 75 at. % for Pt–Cr. Thus, a bcc Cr-base solid solution is formed in both the Ir–Cr and Pt–Cr systems at Cr-rich compositions. This behavior is consistent with the equilibrium phase diagram. A diffraction line at approximately $2\theta_\chi=38°$ ($D_1$) is observed in the Ir–Cr and Pt–Cr systems at Cr contents of 10–70 at and 24–65 at. %, respectively. The $D_1$ peak, similar to the $D_h$ peak, shifts monotonically toward higher angles with increasing Cr content. Note that the $D_1$ peak is not produced by a simple fcc structure.

Structural analysis by TEM was performed to clarify the origin of the $D_1$ diffraction signal. Figure 3 shows cross-sectional TEM images of media prepared using a (a) Pt or (b) $Pt_{40}Cr_{60}$ NMIL. Selected-area diffraction patterns (SADPs) of Pt and $Pt_{40}Cr_{60}$ grains obtained using a 5 nm spot probe beam incident on the (110) plane of the fcc NMIL are also shown. Six diffraction spots, identified as 111, $11\bar{1}$, 002, $\bar{1}\bar{1}\bar{1}$, $\bar{1}\bar{1}1$, and $00\bar{2}$, are observed near the 000 spot in the Pt NMIL, while streaks along the [111] direction can be observed in the $Pt_{40}Cr_{60}$ NMIL. This result indicates that stacking faults

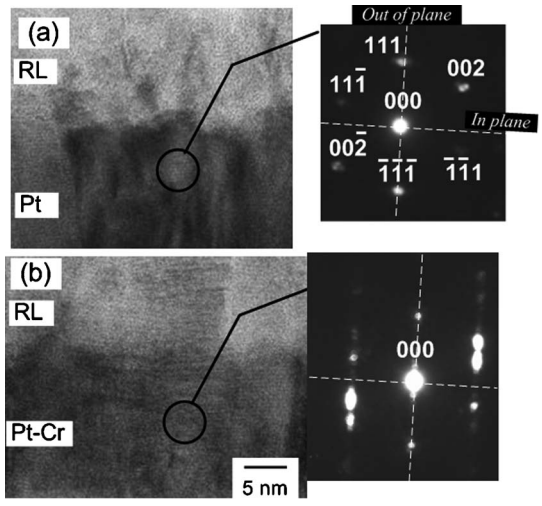


FIG. 3. Cross-sectional TEM images of (a) NiFeCr(20 nm)/Pt(20 nm)/CoPtCr–$SiO_2$(16 nm) and (b) NiFeCr(20 nm)/$Pt_{40}Cr_{60}$(20 nm)/CoPtCr–$SiO_2$(16 nm) films. Right figures show SADPs of the Pt or $Pt_{40}Cr_{60}$ layer.

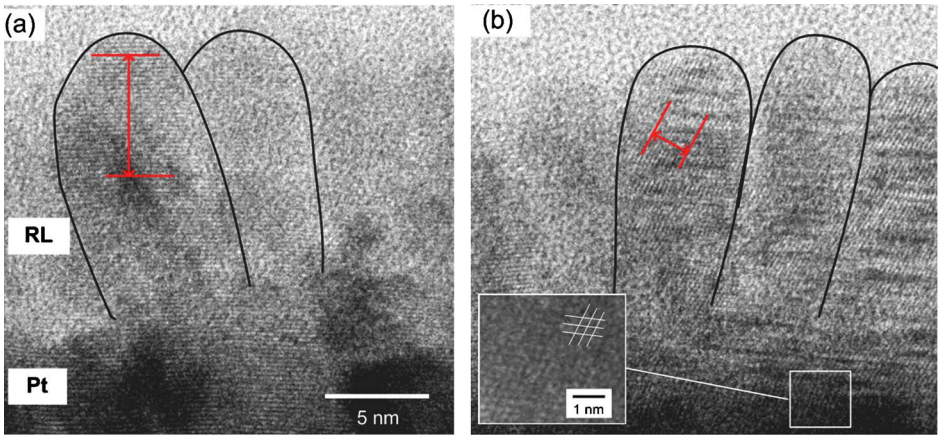


FIG. 4. (Color online) Cross-sectional TEM images for media prepared using a Pt NMIL. (a) Pt grains presenting the [111] axis on the observation plane. (b) Pt grains presenting both [111] and $[11\bar{1}]$ axes.

(SFs) are formed parallel to the (111) plane in the fcc Pt–Cr phase,[5] resulting in streaks crossing the in-plane direction which are not apparent in the simple fcc phase [see Fig. 3(a)]. The lattice spacing analyzed at this cross point is consistent with that indicated by the $D_1$ diffraction in the in-plane XRD profiles. The $D_1$ diffraction therefore appears in the in-plane XRD profiles (Fig. 2) when SFs are present in the (111)-oriented fcc phase. According to the Ir–Cr phase diagram, an $\varepsilon$ phase with hcp structure is formed in the range of 30–60 at. % Cr, where the liquidus and solidus continue from the fcc Ir phase. In this sense, the $D_1$ diffraction can also be identified as the (10.0) plane of the $\varepsilon$ phase with *c*-plane sheet texture. Given the lattice similarity and relationships, that is, $(111)_{\mathrm{fcc}} \| (00.1)_{\mathrm{hcp}}$ and $[\bar{1}\bar{1}0]_{\mathrm{fcc}} \| [10.0]_{\mathrm{hcp}}$, hcp stacking along the [00.1] direction can be regarded as fcc stacking along the [111] direction with periodic SFs.

Comparison of the magnetic properties with the film structures indicates that the compositional ranges of NMIL in which the magnetic properties of the overlying RL are improved (Fig. 1) and where the $D_1$ diffractions appear (Fig. 2) are the same within the Ir–Cr and Pt–Cr systems. This is a common tendency seen for NMILs, not only for the Ir–Cr and Pt–Cr systems but also for Pd–Cr, Au–Cr, Ni–Cr, Ir–Ti, Ir–Nb, and Ir–Zr. It can therefore be concluded that the magnetic properties of a granular RL on a fcc NMIL are improved by the formation of SFs in the fcc NMIL.

The crystal orientation of the magnetic grains grown on the Pt NMIL can be determined from the bright-field cross-sectional TEM images shown in Fig. 4. Lattice stripes in the Pt grains representing the (111) plane [Fig. 4(a)] are oriented parallel to the film plane, as are the lattice stripes in magnetic grains. From the (111)-plane spacing of Pt grains (2.26 Å), the averaged lattice spacing in the hcp magnetic grains is evaluated to be 2.05 Å (average of 30 lattice stripes), which is consistent with the (00.2)-plane spacing measured by XRD. While in another view in TEM image, there exist Pt grains with two types of lattice stripes; one parallel to the film plane, and one oriented ca. 70° from the film normal [see magnified image in Fig. 4(b)], which represents (111) and $(11\bar{1})$ planes, respectively. In the magnetic grains shown in Fig. 4(b), lattice stripes with the 70° orientation can be observed. The average lattice spacing evaluated from ten lattice stripes in magnetic grains is 2.05 Å, which is equivalent to the lattice spacing of magnetic grains in Fig. 4(a). The magnetic grains in Fig. 4(b) therefore have the hcp structure with *c*-plane oriented toward ca. 70° from the film normal. These results suggest that hcp magnetic grains on (111)-oriented Pt grains grow epitaxially on not only the Pt (111) atomic terrace but also the Pt $(\bar{1}11)$, $(1\bar{1}1)$, and $(11\bar{1})$ atomic terraces, which are oriented 70° from the film normal. In the case of the RL on the Pt–Cr NMIL, such obliquely oriented magnetic grains were not observed. It can be easily understood that $K_u^{\mathrm{RL}}$ can be increased if the growth of such obliquely orientated magnetic grains in the RL can be suppressed. The enhancement in $K_u^{\mathrm{RL}}$ by the formation of SFs in fcc NMILs is therefore attributable to the preferred epitaxial growth of magnetic grains on the (111) terrace of the fcc NMIL due to collapse of the sixfold symmetry of the $(\bar{1}11)$, $(1\bar{1}1)$, and $(11\bar{1})$ atomic terraces of the fcc NMIL.

The authors thank Goto of OHARA Inc. for contributing the substrates used in the present experiments.

[1]T. Oikawa, M. Nakamura, H. Uwazumi, T. Shimatsu, and H. Muraoka, IEEE Trans. Magn. **38**, 1976 (2002).
[2]R. Mukai, T. Uzumaki, and A. Tanaka, IEEE Trans. Magn. **41**, 3169 (2005).
[3]W. Y. Lee, M. F. Toney, and D. Mauri, IEEE Trans. Magn. **36**, 381 (2000).
[4]S. Saito, D. Hasegawa, F. Hoshi, D. D. Djayaprawira, and M. Takahashi, Appl. Phys. Lett. **80**, 811 (2002).
[5]B. E. Warren, *X-ray Diffraction* (Addison-Wesley, Reading, MA, 1968), p. 284.